AIAA JOURNAL
Vol. 43, No. 10, October 2005

Energy Optimization in Local Shape Control of Structures with Nonlinear Piezoelectric Actuators

Dongchang Sun* and Liyong Tong†
University of Sydney, Sydney, New South Wales 2006, Australia

Shape control of a local part of a structure rather than the entire structure is often encountered in engineering practice using as less control energy as possible. Energy optimization for local shape control of structures integrated with nonlinear piezoelectric actuators is investigated. The local shape is maintained by assigning the generalized displacements to the desired ones at some given points. The distortion of the residual shape is also limited to a given range. This optimal control voltage distribution is solved by using elimination and the Lagrange multiplier method. A unique solution scheme based on Cholesky decomposition and eigenvalue problem is given to reduce the computational load for finding the Lagrange multipliers from an algebraic equation. The final optimal control voltage distribution for the nonlinear system is obtained by an iteration procedure. Finally, an example is given to illustrate the present method, and the results show that proper relaxation of the error tolerance of the residual shape can significantly reduce the control energy requested for the local shape control of the designated area.

I. Introduction

SHAPE control of flexible structures can be dated back to early 1980s when it was studied to correct any shape distortions of large space structures in space environment.[1] Applications of shape control of structures can be found in large space cranes,[2] large antennas,[3] adaptive mirrors,[4] orbiting platforms,[5] and adaptive variable camber wings.[6] The actuators used in shape control of these space structures are traditional actuators such as point thrust actuators. Since 1985, piezoelectric materials have been widely used as distributed actuators and sensors in active vibration control of structures because of their quick response and light weight. As the improvement of their actuating performance, piezoelectric materials have been increasingly used in shape control of flexible structures, and shape control of structures using linear piezoelectric actuators has been extensively studied[7–14] in recent years.

With increase of the actuating strain of the high-performance piezoelectric materials such as single crystals,[15] the nonlinear constitutive relation inevitably appears particularly when high actuating voltage is applied. Although nonlinear actuation of piezoelectric materials has been referred in some literatures,[16] studies on shape control of structures using nonlinear piezoelectric material as the actuators are very rare. Ajit et al.[17] presented a feedback algorithm to calculate the control voltages required for shape control of a flexible beam using nonlinear piezoelectric actuators. In this algorithm, the difference between the achieved and desired shape is measured in each iterative step, and it is fed back as the new desired shape in the next step to find new control voltages. This iterative process goes on until the measured difference is smaller than the assigned tolerance. Sun et al.[18] presented an iteratively calibrated incremental method to find the optimal control voltages for shape control of plates with nonlinear piezoelectric actuator patches. In this method, the desired shape is expressed by the sum of a number of small incremental desired shapes, and the control voltages to achieve each incremental desired shape are calculated step by step. The control voltages in each step are then calibrated by using the accumulated intermediate desired shape iteratively.

Received 15 January 2004; revision received 28 April 2005; accepted for publication 13 June 2005.

*Research Associate, School of Aerospace, Mechanical and Mechatronic Engineering; dsun@aeromech.usyd.edu.au.

†Professor, School of Aerospace, Mechanical and Mechatronic Engineering. Senior Member AIAA.

In many cases in engineering practice, only a part of an entire structure is needed to maintain a desired shape by making full use of limited control energy. For instance, shape control of an antenna reflector or solar panels in a large space station at a reasonable cost is more practical than the shape control of the whole structures. In this case, the part to be controlled is one of the components of an entire structure, and its governing equation couples with the other parts of the structure. Therefore, local shape control of an entire structure using least control energy is of great importance. In this paper, energy optimization for local shape control of structures integrated with nonlinear piezoelectric actuators is investigated. The local shape is maintained by imposing a linear constraint equation and limiting the distortion of the residual shape to a given tolerance, which leads to a complicated constrained optimization problem. This constrained optimization problem is solved based on direct elimination and the Lagrange multiplier method. A unique solution scheme of an algebraic equation is given to decrease the computational load for finding the Lagrange multipliers, from which optimal control voltages can be found. The final optimal control voltage distribution for the nonlinear system is obtained by an iteration procedure.

II. Basic Equations

A. Description of Nonlinear Piezoelectricity

It is well known that the strain induced by piezoelectric actuators in a piezoelectric actuated structure is very small even when very high driving voltages are applied. In this case, the strain-stress relationship is still in its linear range, whereas the relationship between the induced strain/stress and the driving voltage in piezoelectric materials will be nonlinear. This kind of nonlinear constitutive relation of piezoelectric materials has the following form:

$$\boldsymbol{\sigma} = \boldsymbol{C}\boldsymbol{\varepsilon} - \boldsymbol{\sigma}_p(\boldsymbol{E}) \tag{1}$$

where $\boldsymbol{\sigma} \in R^6$ and $\boldsymbol{\varepsilon} \in R^6$ are the stress and strain vector respectively, $\boldsymbol{C} \in R^{6\times 6}$ is the elastic matrix, and $\boldsymbol{\sigma}_p(\boldsymbol{E}) \in R^6$ is the stress induced by the nonlinear piezoelectricity, which are nonlinear functions of the applied electric field $\boldsymbol{E} \in R^3$. In the following discussion, we assume that the induced stress is a single-valued function of the electric field. Similar to the nonlinear constitutive equation given by Crawley and Lazarus,[19] the nonlinear stress-electric field relation can be rearranged into the following form:

$$\boldsymbol{\sigma}_p(\boldsymbol{E}) = \boldsymbol{e}^T(\boldsymbol{E})\boldsymbol{E} \tag{2}$$

where $\boldsymbol{e}(\boldsymbol{E}) \in R^{3\times 6}$ is the piezoelectric stress coefficient matrix, whose entries are functions of the applied electric field density for nonlinear piezoelectric materials. When the electric field E is applied along the 3 direction, each entry in $\boldsymbol{\sigma}_p$ becomes a function of

E. Employing curve-fitting method, each entry of the piezoelectric stress coefficient matrix can be approximated by

$$e(E) = e_0 + \sum_{k=1}^{K} e_k E^k \tag{3}$$

where $e_k (k = 0, 1, \ldots, K)$ are the coefficients. The coefficients in Eq. (3) can be determined from the test stress-electric field curve by using least-square method.

B. Definition of Generalized Shape

Employing the finite element method, the equilibrium equations of a smart structure with nonlinear piezoelectric actuators can be expressed in the following general form:

$$\boldsymbol{K}\boldsymbol{u} + \boldsymbol{g}(\boldsymbol{v}) = \boldsymbol{f} \tag{4}$$

where $\boldsymbol{K} \in R^{n \times n}$ is the global stiffness matrix, n is the number of the total degrees of freedom (DOF) of the structure, $\boldsymbol{u} \in R^n$ is the displacement vector consisting of all nodal displacements, $\boldsymbol{g}(\boldsymbol{v}) = [g_1(\boldsymbol{v}) \;\; g_2(\boldsymbol{v}) \;\; \cdots \;\; g_n(\boldsymbol{v})]^T$ is the vector of control forces whose components are nonlinear functions of the control voltage, $\boldsymbol{v} \in R^{n_V}$ is the voltage vector composed of all nodal voltage of the piezoelectric actuators, n_V is the total number of the electric DOF and $\boldsymbol{f} \in R^n$ is the force vector contributed by all mechanical loads. As a special case where the control voltage is uniformly applied on each piezoelectric actuator, the number of electric DOF is equal to that of the piezoelectric actuators.

In general, the desired shape of a structure might not be exactly achieved because the number of the input control voltages is much less than that of the total mechanical DOF. Therefore, the shape control is usually performed by finding the optimal control voltages, which minimizes the defined error between the actuated shape and the desired one. There can be various error functions defined for different emphases in static shape control, which depends on the definition of the shape function. A given shape of a structure is usually described by its displacements from a selected reference system. However, in some special cases the objective of shape control of a structure can involve slope and curvature,[20] strain, or even generalized forces in addition to the pure displacements. Therefore, a generalized shape should be defined to include all of this information. To this end, we consider a generalized "shape" defined by

$$\boldsymbol{y} = \boldsymbol{R}_d\boldsymbol{u} + \boldsymbol{R}_c\boldsymbol{\chi} + \boldsymbol{R}_s\boldsymbol{\varepsilon} + \boldsymbol{R}_g\boldsymbol{f}_g \tag{5}$$

where $\boldsymbol{y} \in R^m$ is an index vector of the generalized shape; $\boldsymbol{u}$, $\boldsymbol{\chi}$, $\boldsymbol{\varepsilon}$, and $\boldsymbol{f}_g$ are displacements including translational displacements and rotational angles (slopes), curvatures, strains and generalized forces respectively; and $\boldsymbol{R}_d$, $\boldsymbol{R}_c$, $\boldsymbol{R}_s$, and $\boldsymbol{R}_g$ are the corresponding weighting matrices. Because the curvatures, strains, and generalized force of a structure can be expressed in term of the displacements $\boldsymbol{\chi} = \boldsymbol{B}_c\boldsymbol{u}$, $\boldsymbol{\varepsilon} = \boldsymbol{B}_s\boldsymbol{u}$, $\boldsymbol{f}_g = \boldsymbol{K}_g\boldsymbol{u}$ in which $\boldsymbol{B}_c$, $\boldsymbol{B}_s$, and $\boldsymbol{K}_g$ are coefficient matrices for curvatures, strains, and generalized forces, respectively, the multiobjective shape $\boldsymbol{y}$ in Eq. (5) can be finally written in the following form:

$$\boldsymbol{y} = \boldsymbol{R}\boldsymbol{u} \tag{6}$$

where $\boldsymbol{R} \in R^{m \times n}$ is the overall weighting matrix given by

$$\boldsymbol{R} = \boldsymbol{R}_d + \boldsymbol{R}_c\boldsymbol{B}_c + \boldsymbol{R}_s\boldsymbol{B}_s + \boldsymbol{R}_g\boldsymbol{K}_g \tag{7}$$

In this case, for a desired shape $\boldsymbol{y}_d$, we can define the error function between the actuated and the desired shapes as

$$e = |\boldsymbol{y} - \boldsymbol{y}_d|^2 = (\boldsymbol{y} - \boldsymbol{y}_d)^T(\boldsymbol{y} - \boldsymbol{y}_d) \tag{8}$$

A part of the generalized displacement $\boldsymbol{u}_1$ can be used to describe a local shape of a structure. More generally, a weighted displacement vector is used:

$$\boldsymbol{y}_1 = \boldsymbol{R}_1\boldsymbol{u} = \boldsymbol{y}_{1d} \tag{9}$$

where $\boldsymbol{y}_1 \in R^{n_1}$ is a vector to be constrained, which can also include some nodal displacements, rotational angle, curvatures or their combinations depending on the selection of the weighting matrix, $\boldsymbol{R}_1 \in R^{n_1 \times n}$, and $\boldsymbol{y}_{1d}$ is the desired value of the vector $\boldsymbol{y}_1$. The number of the constraining equation n_1 should be less than the number of the control inputs n_V so that the control voltages that satisfy Eq. (9) exist.

Because the control energy consumed by piezoelectric actuators can be expressed as

$$\sum_{i=1} z_i V_i^2$$

where z_i is a constant representing capacitance, the total control energy can be defined as

$$E = \boldsymbol{v}^T\boldsymbol{Z}\boldsymbol{v} \tag{10}$$

where $\boldsymbol{Z} \in R^{n_V \times n_V}$ is a diagonal weighting matrix representing capacitance. To avoid the unlimitedly increase of the energy with the node number of the piezoelectric actuator elements, an average energy level is defined as follows:

$$\bar{E} = \boldsymbol{v}^T\boldsymbol{Z}\boldsymbol{v}/n_V = \boldsymbol{v}^T\bar{\boldsymbol{Z}}\boldsymbol{v}, \qquad \bar{\boldsymbol{Z}} = \boldsymbol{Z}/n_V \tag{11}$$

The average energy will be used as the objective function to find the optimal control voltages for shape control in the following sections.

III. Optimization of Control Energy Under Constraints

The objective of the optimization is finding the optimal control voltages for the nonlinear piezoelectric actuators to minimize consumption of the control energy under the following two constraints: 1) some local shapes should be satisfied (i.e., the displacements of the assigned nodes, which control some local shapes, are made equal to the desired ones), and 2) the error between the other shapes and their corresponding desired shapes falls in a given range. The optimization can be stated as follows.

Min:

$$\bar{E} = \boldsymbol{v}^T\bar{\boldsymbol{Z}}\boldsymbol{v}$$

Subject to:

$$\boldsymbol{y}_1 = \boldsymbol{R}_1\boldsymbol{u} = \boldsymbol{y}_{1d}$$

$$e = (\boldsymbol{y} - \boldsymbol{y}_d)^T(\boldsymbol{y} - \boldsymbol{y}_d) \le e_0 \tag{12a}$$

where e_0 is the assigned error tolerance. Because the second constraint in Eq. (12a) is an inequality, to seek the solution of Eq. (12a) we first consider the problem with an equality constraint as follows.

Min:

$$\boldsymbol{v}^T\bar{\boldsymbol{Z}}\boldsymbol{v}$$

Subject to:

$$\boldsymbol{R}_1\boldsymbol{u} = \boldsymbol{y}_{1d}$$

$$(\boldsymbol{y} - \boldsymbol{y}_d)^T(\boldsymbol{y} - \boldsymbol{y}_d) = e_0 \tag{12b}$$

and then find the solution of the original problem in Eq. (12a) via monotony analysis.

The two constraining equations in Eq. (12b) can be combined into one equation by elimination. The relationship between the displacement and the control voltage can be expressed from Eq. (4) as

$$\boldsymbol{u} = \boldsymbol{K}^{-1}\boldsymbol{f} - \boldsymbol{K}^{-1}\boldsymbol{g}(\boldsymbol{v}) \tag{13}$$

Because the control forces in $\boldsymbol{g}(\boldsymbol{v})$ are nonlinear functions of the control voltage vector $\boldsymbol{v}$, the solution of Eq. (12b) has to be sought iteratively. To this end, nonlinear control force vector $\boldsymbol{g}(\boldsymbol{v})$ in Eq. (4) can be linearized by minimizing the error $\boldsymbol{g}(\boldsymbol{v}) - \boldsymbol{G}\boldsymbol{v}$. From $(\partial/\partial\boldsymbol{v})[\boldsymbol{g}(\boldsymbol{v}) - \boldsymbol{G}\boldsymbol{v}] = \boldsymbol{0}$, the equivalent actuating matrix $\boldsymbol{G}$ can be obtained by

$$\boldsymbol{G} = \frac{\partial \boldsymbol{g}(\boldsymbol{v})}{\partial \boldsymbol{v}} \tag{14}$$

where $\boldsymbol{G} \in R^{n \times n_V}$ is the Jacobian matrix, and it will be taken as a constant matrix in each iteration step although it is actually a function of $\boldsymbol{v}$.

Substituting Eqs. (13) and (14) into Eq. (9) gives

$$\bar{\boldsymbol{R}}_1\boldsymbol{v} = \bar{\boldsymbol{y}}_{1d}$$

$$\bar{\boldsymbol{R}}_1 = \boldsymbol{R}_1\boldsymbol{K}^{-1}\boldsymbol{G} \in R^{n_1 \times n_V}, \qquad \bar{\boldsymbol{y}}_{1d} = \boldsymbol{R}_1\boldsymbol{K}^{-1}\boldsymbol{f} - \boldsymbol{y}_{1d} \in R^{n_1} \quad (15)$$

Because of the n_1 constraining equations in Eq. (9), the total number of independent design voltages will be reduced from n_V to $n_V - n_1$. We separate the control voltages into two parts: one is to be eliminated, and the other will be retained. The voltage vector can be rearranged as

$$\boldsymbol{v} = [\boldsymbol{T}_e \quad \boldsymbol{T}_r]\begin{Bmatrix}\boldsymbol{v}_e \\ \boldsymbol{v}_r\end{Bmatrix} = \boldsymbol{T}_e\boldsymbol{v}_e + \boldsymbol{T}_r\boldsymbol{v}_r \quad (16)$$

where $\boldsymbol{T}_e \in R^{n_V \times n_1}$ and $\boldsymbol{T}_r \in R^{n_V \times (n_V - n_1)}$ are transformation matrices. Substituting Eq. (16) into Eq. (15), we have

$$\boldsymbol{R}_e\boldsymbol{v}_e + \boldsymbol{R}_r\boldsymbol{v}_r = \bar{\boldsymbol{y}}_{1d}, \qquad \boldsymbol{R}_e = \bar{\boldsymbol{R}}_1\boldsymbol{T}_e \in R^{n_1 \times n_1}$$

$$\boldsymbol{R}_r = \bar{\boldsymbol{R}}_1\boldsymbol{T}_r \in R^{n_1 \times (n_V - n_1)} \quad (17)$$

If the elements of $\boldsymbol{v}_e$ are properly selected so that $\boldsymbol{R}_e$ is nonsingular and $\boldsymbol{v}_e$ can be expressed by $\boldsymbol{v}_r$,

$$\boldsymbol{v}_e = \boldsymbol{R}_e^{-1}(\bar{\boldsymbol{y}}_{1d} - \boldsymbol{R}_r\boldsymbol{v}_r) \quad (18)$$

Substituting Eq. (16) into Eq. (11), the average control energy can be written as

$$\bar{E} = \boldsymbol{v}_e^T\boldsymbol{T}_e^T\bar{\boldsymbol{Z}}\boldsymbol{T}_e\boldsymbol{v}_e + 2\boldsymbol{v}_r^T\boldsymbol{T}_r^T\bar{\boldsymbol{Z}}\boldsymbol{T}_e\boldsymbol{v}_e + \boldsymbol{v}_r^T\boldsymbol{T}_r^T\bar{\boldsymbol{Z}}\boldsymbol{T}_r\boldsymbol{v}_r \quad (19)$$

Eliminating $\boldsymbol{v}_e$ from Eq. (19) by using Eq. (18) yields

$$\bar{E} = c_E + 2\boldsymbol{b}_E^T\boldsymbol{v}_r + \boldsymbol{v}_r^T\boldsymbol{A}_E\boldsymbol{v}_r \quad (20)$$

where

$$\boldsymbol{A}_E = \left(\boldsymbol{T}_r - \boldsymbol{T}_e\boldsymbol{R}_e^{-1}\boldsymbol{R}_r\right)^T\bar{\boldsymbol{Z}}\left(\boldsymbol{T}_r - \boldsymbol{T}_e\boldsymbol{R}_e^{-1}\boldsymbol{R}_r\right)$$

$$\boldsymbol{b}_E^T = \bar{\boldsymbol{y}}_{1d}^T\boldsymbol{R}_e^{-T}\boldsymbol{T}_e^T\bar{\boldsymbol{Z}}\left(\boldsymbol{T}_r - \boldsymbol{T}_e\boldsymbol{R}_e^{-1}\boldsymbol{R}_r\right), \qquad c_E = \bar{\boldsymbol{y}}_{1d}^T\boldsymbol{R}_e^{-T}\boldsymbol{T}_e^T\bar{\boldsymbol{Z}}\boldsymbol{T}_e\boldsymbol{R}_e^{-1}\bar{\boldsymbol{y}}_{1d} \quad (21)$$

The square error defined in Eq. (8) can also be expressed by the control voltage $\boldsymbol{v}$. Substituting the linearized Eq. (13) into Eq. (8), we have

$$e = \bar{\boldsymbol{y}}_d^T\bar{\boldsymbol{y}}_d - 2\bar{\boldsymbol{y}}_d^T\boldsymbol{P}\boldsymbol{v} + \boldsymbol{v}^T\boldsymbol{P}^T\boldsymbol{P}\boldsymbol{v}$$

$$\bar{\boldsymbol{y}}_d = \boldsymbol{R}\boldsymbol{K}^{-1}\boldsymbol{f} - \boldsymbol{y}_d, \qquad \boldsymbol{P} = \boldsymbol{R}\boldsymbol{K}^{-1}\boldsymbol{G} \quad (22)$$

Substituting Eq. (18) into Eq. (22) gives

$$e = c_e + 2\boldsymbol{b}_e^T\boldsymbol{v}_r + \boldsymbol{v}_r^T\boldsymbol{A}_e\boldsymbol{v}_r \quad (23)$$

where

$$c_e = \left(\bar{\boldsymbol{y}}_d - \boldsymbol{P}\boldsymbol{T}_e\boldsymbol{R}_e^{-1}\bar{\boldsymbol{y}}_{1d}\right)^T\left(\bar{\boldsymbol{y}}_d - \boldsymbol{P}\boldsymbol{T}_e\boldsymbol{R}_e^{-1}\bar{\boldsymbol{y}}_{1d}\right)$$

$$\boldsymbol{b}_e^T = -\left(\bar{\boldsymbol{y}}_d - \boldsymbol{P}\boldsymbol{T}_e\boldsymbol{R}_e^{-1}\bar{\boldsymbol{y}}_{1d}\right)^T\boldsymbol{P}\left(\boldsymbol{T}_r - \boldsymbol{T}_e\boldsymbol{R}_e^{-1}\boldsymbol{R}_r\right)$$

$$\boldsymbol{A}_e = \left(\boldsymbol{T}_r - \boldsymbol{T}_e\boldsymbol{R}_e^{-1}\boldsymbol{R}_r\right)^T\boldsymbol{P}^T\boldsymbol{P}\left(\boldsymbol{T}_r - \boldsymbol{T}_e\boldsymbol{R}_e^{-1}\boldsymbol{R}_r\right) \quad (24)$$

After eliminating $\boldsymbol{v}_e$, the optimization problem described in Eq. (12b) can be transformed into the following form.

Min:

$$c_E + 2\boldsymbol{b}_E^T\boldsymbol{v}_r + \boldsymbol{v}_r^T\boldsymbol{A}_E\boldsymbol{v}_r$$

Subject to:

$$c_e + 2\boldsymbol{b}_e^T\boldsymbol{v}_r + \boldsymbol{v}_r^T\boldsymbol{A}_e\boldsymbol{v}_r = e_0 \quad (25)$$

To find the solution of Eq. (25), we construct a function as

$$F(\boldsymbol{v}_r, \lambda) = c_E + 2\boldsymbol{b}_E^T\boldsymbol{v}_r + \boldsymbol{v}_r^T\boldsymbol{A}_E\boldsymbol{v}_r + \lambda\left(c_e + 2\boldsymbol{b}_e^T\boldsymbol{v}_r + \boldsymbol{v}_r^T\boldsymbol{A}_e\boldsymbol{v}_r - e_0\right) \quad (26)$$

where λ is the Lagrange's multiplier. The optimal value of $\boldsymbol{v}_r$ can be found by

$$\frac{\partial F}{\partial \boldsymbol{v}_r} = 0, \qquad \frac{\partial F}{\partial \lambda} = 0 \quad (27)$$

which lead to the following equations:

$$(\boldsymbol{A}_E + \lambda\boldsymbol{A}_e)\boldsymbol{v}_r + \boldsymbol{b}_E + \lambda\boldsymbol{b}_e = 0$$

$$c_e + 2\boldsymbol{b}_e^T\boldsymbol{v}_r + \boldsymbol{v}_r^T\boldsymbol{A}_e\boldsymbol{v}_r = e_0 \quad (28)$$

As a direct way of solving Eq. (28), substituting

$$\boldsymbol{v}_r = -(\boldsymbol{A}_E + \lambda\boldsymbol{A}_e)^{-1}(\boldsymbol{b}_E + \lambda\boldsymbol{b}) \quad (29)$$

into the second equation (28) gives

$$c_e - 2\boldsymbol{b}_e^T(\boldsymbol{A}_E + \lambda\boldsymbol{A}_e)^{-1}(\boldsymbol{b}_E + \lambda\boldsymbol{b}) + (\boldsymbol{b}_E + \lambda\boldsymbol{b})^T(\boldsymbol{A}_E + \lambda\boldsymbol{A}_e)^{-T}$$

$$\times\boldsymbol{A}_e(\boldsymbol{A}_E + \lambda\boldsymbol{A}_e)^{-1}(\boldsymbol{b}_E + \lambda\boldsymbol{b}) = e_0 \quad (30)$$

Equation (30) is an algebraic equation of λ, and its roots can be found by some numerical methods such as the secant method and Newton–Raphson method. After solving the Lagrangian multipliers λ from Eq. (30) and substituting them into Eq. (29), the retained control voltage $\boldsymbol{v}_r$ can be obtained. However, finding the roots of Eq. (30) is very time consuming because the inverse of matrix $(\boldsymbol{A}_E + \lambda\boldsymbol{A}_e)$ has to be calculated for different value of λ in the iterative root seeking process.

To reduce the computation for finding the Lagrangian multipliers, complicated calculations related to matrices whose entries depend on λ should be avoided. As shown in Eq. (24), $\boldsymbol{A}_e$ is a symmetric positive-definite matrix, and it can be expressed as (Cholesky decomposition)

$$\boldsymbol{A}_e = \boldsymbol{\Psi}_e\boldsymbol{\Psi}_e^T \quad (31)$$

where $\boldsymbol{\Psi}_e \in R^{(n_V - n_1)\times(n_V - n_1)}$ is a lower triangular matrix with positive diagonal entries. Taking transformation

$$\boldsymbol{v}_r = \boldsymbol{\Psi}_e^{-T}\bar{\boldsymbol{v}}_r \quad (32)$$

in Eq. (28) and noting Eq. (31), Eq. (28) can be transformed into the following form:

$$\bar{\boldsymbol{A}}_E\bar{\boldsymbol{v}}_r + \lambda\bar{\boldsymbol{v}}_r + \bar{\boldsymbol{b}}_E + \lambda\bar{\boldsymbol{b}}_e = 0, \qquad c_e + 2\bar{\boldsymbol{b}}_e^T\bar{\boldsymbol{v}}_r + \bar{\boldsymbol{v}}_r^T\bar{\boldsymbol{v}}_r = e_0 \quad (33)$$

where

$$\bar{\boldsymbol{A}}_E = \boldsymbol{\Psi}_e^{-1}\boldsymbol{A}_E\boldsymbol{\Psi}_e^{-T}, \qquad \bar{\boldsymbol{b}}_E = \boldsymbol{\Psi}_e^{-1}\boldsymbol{b}_E, \qquad \bar{\boldsymbol{b}}_e = \boldsymbol{\Psi}_e^{-1}\boldsymbol{b}_e \quad (34)$$

It can be seen from Eqs. (21) and (34) that $\bar{\boldsymbol{A}}_E$ keeps symmetric after transformation.

Denoting α_i and φ_i $(i = 1, 2, \ldots, n_V - n_1)$ as the ith eigenvalue and corresponding eigenvector of matrix $\bar{\boldsymbol{A}}_E$ and expressing $\bar{\boldsymbol{v}}_r, \bar{\boldsymbol{b}}_E$, and $\bar{\boldsymbol{b}}_e$ as

$$\bar{\boldsymbol{v}}_r = \sum_{i=1}^{n_V - n_1}\beta_i\varphi_i, \qquad \bar{\boldsymbol{b}}_E = \sum_{i=1}^{n_V - n_1}\gamma_i\varphi_i, \qquad \bar{\boldsymbol{b}}_e = \sum_{i=1}^{n_V - n_1}\xi_i\varphi_i \quad (35)$$

Eq. (33) can become

$$\sum_{i=1}^{n_V - n_1}(\alpha_i\beta_i + \lambda\beta_i + \gamma_i + \lambda\xi_i)\varphi_i = 0$$

$$\sum_{i=1}^{n_V - n_1}\left(\beta_i^2 + 2\xi_i\beta_i\right) = e_0 - c_e \quad (36)$$

β_i can be solved from the first equation (36) as

$$\beta_i = -\frac{\gamma_i + \lambda\xi_i}{\alpha_i + \lambda}, \qquad i = 1, 2, \ldots, n_V - n_1 \quad (37)$$

Substituting Eq. (37) into the second equation, we have

$$\sum_{i=1}^{n_V-n_1}\left[\left(\frac{\gamma_i+\lambda\xi_i}{\alpha_i+\lambda}\right)^2-2\xi_i\frac{\gamma_i+\lambda\xi_i}{\alpha_i+\lambda}\right]=e_0-c_e \tag{38}$$

which is an explicit algebraic equation of λ and can be solved much more easily than Eq. (30). For each λ solved from Eq. (38), we can obtain a control voltage distribution $\boldsymbol{v}$ by using Eqs. (16), (18), (32), (33), and (37) sequentially. Equation (38) has $2(n_V-n_1)$ roots, but only the real ones can lead to rational control voltage distributions. When the desired error e_0 is too small, Eq. (38) will not have a real root, which reflects that this desired error cannot be implemented. On the contrary, when a big e_0 is given, Eq. (38) can have more than one real root, each of which gives a control voltages distribution that can make the error equal to the given one. In this case, only the one with least control energy is our desired solution.

As a special case, if there is no constraint on the square error, that is, $\lambda=0$ in Eq. (29), the obtained control voltages become

$$\boldsymbol{v}_{r\,\mathrm{lst}}=-\boldsymbol{A}_E^{-1}\boldsymbol{b}_E \tag{39}$$

Equation (39) together with Eq. (18) gives the control voltage distribution $\boldsymbol{v}_{\mathrm{lst}}$ with least control energy E_{lst} that actuates a shape possessing the given values at the assigned nodes. In this case, the square error between the shape actuated by $\boldsymbol{v}_{\mathrm{lst}}$ and the desired one is denoted by e_{lst}, which is usually much larger than the possibly achieved minimum error $e_{\min}$.

In addition, to give suitable square error in the constraining equation, we need to know the smallest square error $e_{\min}$ that can be implemented by the best control voltage distribution. Such a control voltage distribution can be obtained by minimizing the square error in Eq. (8) and the constraint in Eq. (9). After eliminating n_1 voltages, the square error can be transformed to the form given in Eq. (23), and therefore, we have

$$\min \qquad e=c_e+2\boldsymbol{b}_e^T\boldsymbol{v}_r+\boldsymbol{v}_r^T\boldsymbol{A}_e\boldsymbol{v}_r \tag{40}$$

from which we can easily find the optimal control voltage as

$$\boldsymbol{v}_{r\,\min}=-\boldsymbol{A}_e^T\boldsymbol{b}_e \tag{41}$$

Once the optimal control voltage distribution is found, a new equivalent actuating matrix $\boldsymbol{G}$ in Eq. (14) is recalculated at the new voltage distribution. Repeating the process of finding the optimal control voltages, the final optimal control voltage distribution for a nonlinear system can be obtained iteratively, as shown in Fig. 1.

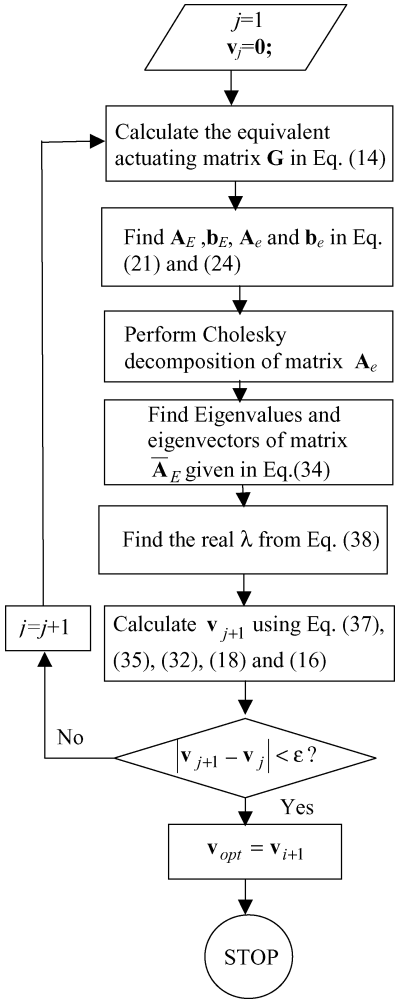

Fig. 1 Flowchart of the iteration process for finding the optimal control voltage distribution.

IV. Illustrative Examples

As an illustrative example, consider a rectangular thin plate in a horizontal plane that is clamped at its left edge. There are 30 nonlinear piezoelectric actuator patches bonded on the upper surface of the host plate, which are made of lead zirconate titanate (PZT) and have the same physical properties and geometric dimensions, as shown in Fig. 2. The dimensions of each piezoelectric patch are 2 cm × 2 cm × 0.5 mm. The host plate is 0.15 m long, 0.12 m wide, and 0.001 m thick. The gap between any two piezoelectric actuator patches is 0.5 cm, and that between the clamped side and the actuator in the left column is also 0.5 mm. The physical properties of the host plate are $c_{11}=c_{22}=73.49$ GPa, $c_{12}=18.37$ GPa, $c_{66}=27.56$ GPa, and $c_{13}=c_{23}=0$. The piezoelectric material has the following properties: $c_{11}=c_{22}=99.74$ GPa, $c_{12}=42.89$ GPa, and $c_{66}=28.43$ GPa. The adhesive layer between the piezoelectric actuators and the host plate has a thickness of 0.15 mm, and its material properties are $c_a=3.69$ GPa and $G_{1a}=G_{2a}=0.896$ GPa. The mass densities of the host plate, piezoelectric material, and the adhesive layer are 2700, 7600, and 1600 kg/m^3, respectively.

The control voltage is uniformly distributed in each piezoelectric actuator patch. Without loss of generality, the capacitance z of each piezoelectric patch is assumed to be 1.0. Because of the nonlinearity of the piezoelectricity, the piezoelectric stress modulus of the piezoelectric material is a function of the applied control voltage (field) as described by

$$e_{31}(V)=e_{32}(V)=e_{310}[1+\alpha\,\mathrm{sgn}(V)V]$$

where the parameter α is a nonlinear factor, which determines the shape of the nonlinear stress-voltage curve. A negative nonlinear factor α represents a softening nonlinear stress-voltage relationship. When $e_0=9.53$ N/Vm, α is taken as -2×10^{-5}, -2.5×10^{-5}, -2.8×10^{-5}, and -3×10^{-5}, respectively; the relationship between the induced stress and the applied control voltage is shown in Fig. 3.

To establish the relationship between the control voltages and the displacements of the composite plate, the finite element method can be used to form its equilibrium equations. As shown in Fig. 4, an eight-node adhesive element,[18] which includes the four-node quadrilateral upper (piezoelectric material) and lower plate elements as well as the thin adhesive layer element between them, is employed to model the plate bonded with piezoelectric actuator, whereas an ordinary four-node plate element is used to model host plate itself. In the adhesive element, both peel and shear effects in the adhesive layer are modeled based on the first-order shear deformation plate theory. The composite plate is divided into 78 ordinary plate elements and 30 adhesive elements. The total number of nodes is 250, as shown in Fig. 2. In each node, there are five mechanical DOF and one electric DOF (electric field). After deducting the constrained DOFs, there are totally 1200 independent mechanical DOFs and 30 electric DOFs in this example, that is, $n=1200$ and $n_V=30$.

In this example, the weighting matrix $\boldsymbol{R}$ is chosen in such a way that the weighting coefficients corresponding to the transverse displacements, the rotation angle about x axis, and the rotation angle about y axis at all nodes of the host plate are 1.0, 0.02, and 0.002, respectively.

In this example, the desired shape is simply a flat one in a horizontal plane, which can be expressed as $w_d(x,y)=0$. The shape

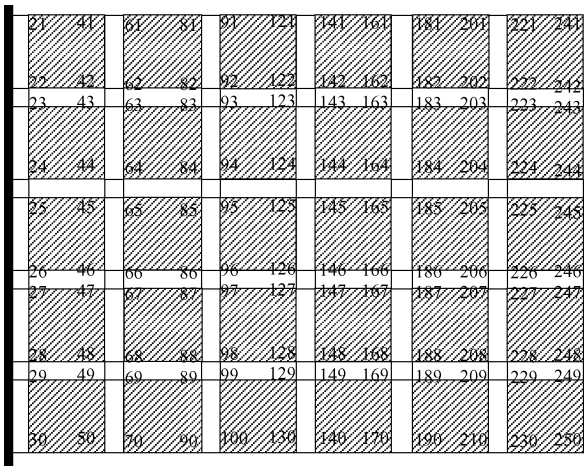

a) Top view of a cantilever plate with 30 piezoelectric patches

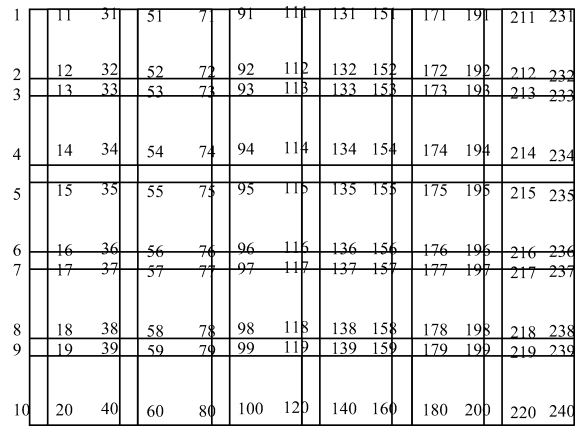

b) Host plate with nodal numbers

Fig. 2 Cantilever plate with 30 piezoelectric actuator patches.

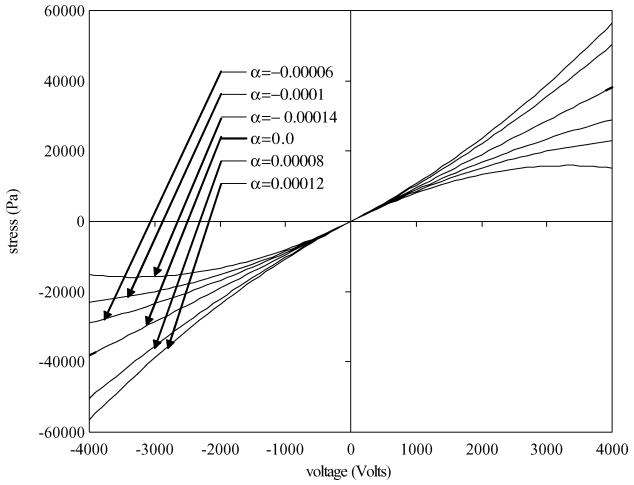

Fig. 3 Nonlinear constitutive relation between the stress and electric field of the piezoelectric material.

at the free end of the plate is of particular interest and should be implemented as close as possible to the desired shape with minimum control energy and the total square error is limited to a given range. To this end, we choose the transverse displacements at node 211, 213, 215, 217, 219, 220, 231, 232, 234, 236, 238, and 240, which will be made exactly the same as the desired values. When $e_{310} = 9.53$ N/Vm, the nonlinear factor α is 0.000035, and the given square error e_0 is 1.25×10^{-8} m^2; the optimal control voltages can be obtained from Eq. (12b) iteratively. In the calculation, four real Lagrange multipliers were found from Eq. (38), which means that

Table 1 Four possible control voltage distributions

Parameter	1 (possible distribution)	2 (possible distribution)	3 (possible distribution)	4 (actual distribution)
Voltage	−1243.23	504.041	−456.976	−499.816
	−179.356	−1317.55	−1348.95	−1119.34
	−2322.95	−1564.5	−1592.67	−1381.56
	−165.768	−971.585	−987.69	−1063.69
	−1233.51	−735.478	−702.654	−374.235
	−1780.18	−1296.18	−1358.09	−630.927
	1433.08	−233.995	−129.918	−547.564
	−2229.87	591.851	549.536	−561.928
	1488.07	−1115.03	−1142.89	−566.564
	−1803.47	−618.538	−577.144	−680.035
	−1693.93	−1142.54	−1069.98	−512.378
	1836.75	70.7752	−33.7355	−261.769
	−2328.15	157.754	175.402	−168.687
	2034.39	−406.418	−362.64	−366.935
	−1829.34	−778.3	−825.817	−835.787
	−1141.59	32.2787	124.883	−337.273
	1627.66	−967.063	−1060.07	−130.633
	−1847.25	1064.15	973.841	51.4942
	2080.66	81.7744	285.959	−162.897
	−1720.04	−587.698	−653.082	−1298.04
	−741.167	−827.797	−833.099	−689.308
	447.858	559.476	565.498	408.05
	−1061.54	−1378.09	−1365.28	−617.163
	815.574	1092.4	1048.98	745.395
	−1058.68	−1650.81	−1627.08	−430.809
	168.786	217.527	213.877	133.366
	291.114	247.952	252.37	341.011
	576.032	726.522	714.176	460.596
	56.1625	−118.55	−102.494	156.611
	572.897	954.467	926.121	303.458
Average control energy $\bar{E}$	2.0808×10^{6}	7.5127×10^{5}	7.5121×10^{5}	3.91474×10^{5}
Square error	1.25×10^{-8}	1.25×10^{-8}	1.25×10^{-8}	1.25×10^{-8}

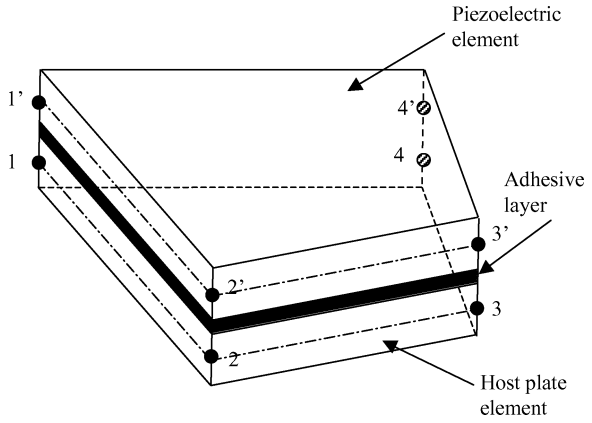

Fig. 4 Eight-node adhesive element.

function $F(\boldsymbol{v}_r, \lambda)$ has four extrema achieved by control voltage distribution respectively. These four real Lagrange multipliers lead to four possible control voltage distributions, as listed in Table 1, which can achieve the shapes and satisfy the given constraints. The average control energy for these four control voltage distributions is 2.0808×10^6, 7.5127×10^5, 7.5121×10^5, and 3.9147×10^5 J, respectively. The first three voltage distributions can achieve the desired shape at the given square error using much more control energy than the fourth one. Clearly, the optimal control voltage distribution is that with the minimum control energy, that is, 3.9147×10^5 J. The maximum control voltage in the optimal voltage distribution is 1381 V. In engineering practice, because very high control voltage can result in electric breakdown of the actuator, voltage limitation should be imposed.

The shape actuated by the optimal control voltages is shown in Fig. 5a, in which the uncontrolled shape of the plate caused by the

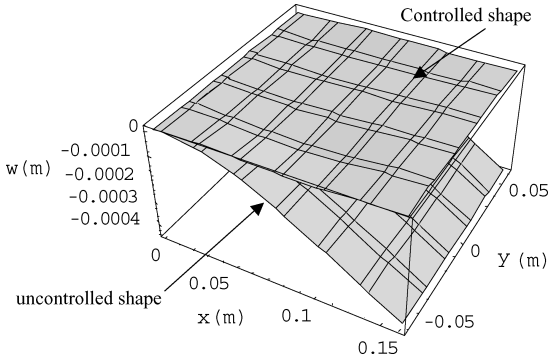

a) Controlled and uncontrolled shapes

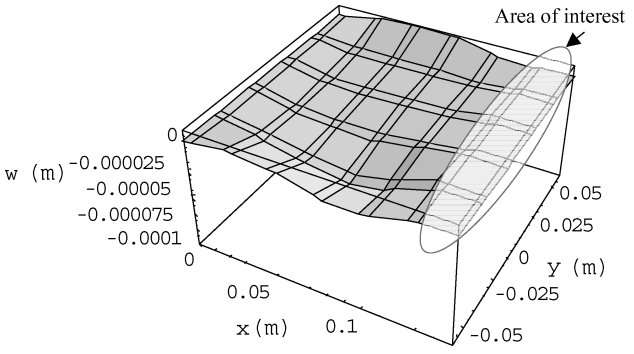

b) Enlarged view of the controlled shape

Fig. 5 Controlled shape achieved under constraints.

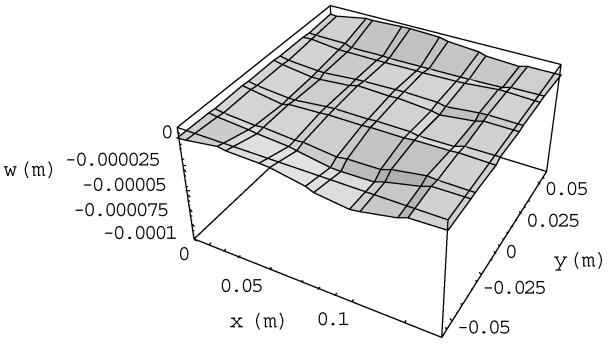

a) $e_0 = 7 \times 10^{-9}$, control energy: 479,459 J

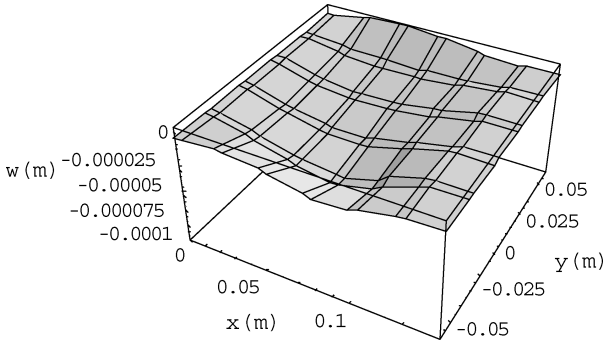

d) $e_0 = 20 \times 10^{-9}$, control energy: 366,825 J

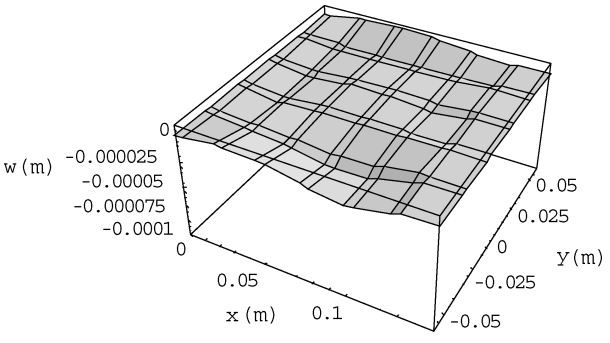

b) $e_0 = 9 \times 10^{-9}$, control energy: 422,708 J

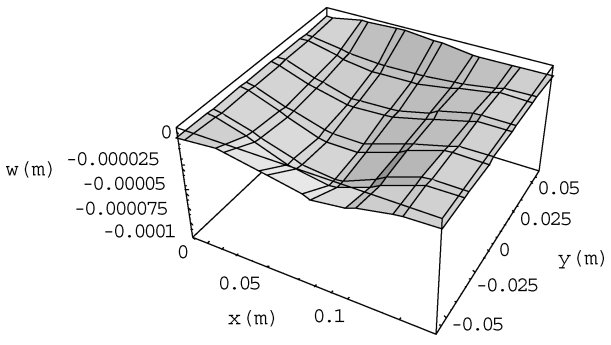

e) $e_0 = 30 \times 10^{-9}$, control energy: 357,915 J

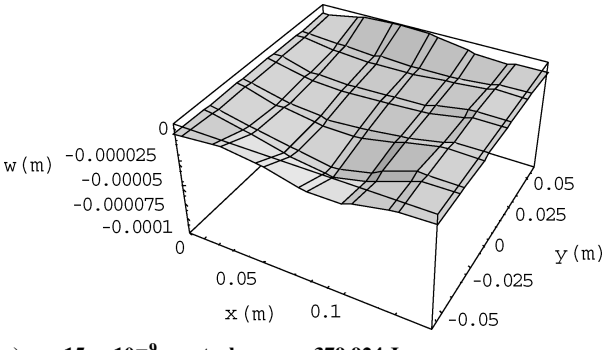

c) $e_0 = 15 \times 10^{-9}$, control energy: 379,924 J

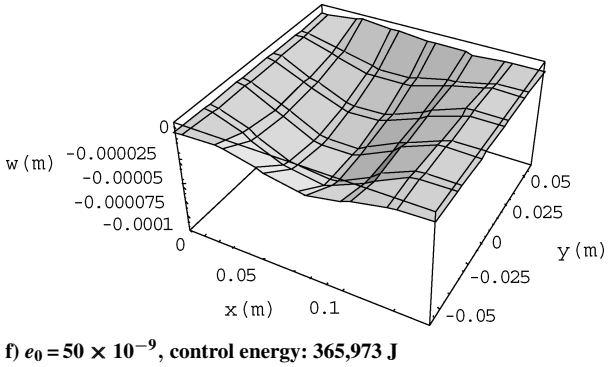

f) $e_0 = 50 \times 10^{-9}$, control energy: 365,973 J

Fig. 6 Actuated shapes by imposing different constraints on square error.

gravity is also given. Compared to the controlled and uncontrolled shape, it can be found that the controlled shape is very close to the desired one. Because the constraints on the transverse displacements at node 211, 213, 215, 217, 219, 220, 231, 232, 234, 236, 238, and 240 are imposed, the transverse displacements at these nodes exactly equal the desired ones, and, therefore, the actuated shape at the right end of the plate is much closer to the desired one than other parts, as shown in Fig. 5b.

Figure 6 shows that achieved shapes when square error e_0 are chosen as 7×10^{-9}, 9×10^{-9}, 15×10^{-9}, 20×10^{-9}, 30×10^{-9}, and 50×10^{-9}, respectively. As shown in Fig. 6, the closeness between the actuated and the desired shape depends on the selection of the assigned square error e_0. When choosing a smaller square error, a shape that is closer to the desired one can be obtained, but the control energy of the obtained optimal control voltages is higher. However, no matter what square error is assigned, the right part of

the actuated shape is always very close to the desired ones because of the constraints on the transverse displacements in this area.

Next, we examine the relationship between the control energy and the assigned square error for different nonlinear factors. The minimum square error achieved by the optimal control voltages obtained from Eq. (41) is a constant, that is, $e_{\min} = 6.5503 \times 10^{-9}$ m^2, although the control voltages are different for different nonlinear factor α. If a square error e_0 smaller than $e_{\min}$ is given in Eq. (12b), no real Lagrange multipliers can be found from Eq. (38), and therefore no control voltage distribution can be found to implement such a square error. When the constraining square errors are chosen as 7×10^{-9}, 9×10^{-9}, 12.5×10^{-9}, 15×10^{-9}, 20×10^{-9}, 30×10^{-9}, 50×10^{-9}, and 70×10^{-9}, the relationship between the least control energy and the assigned square error for different nonlinear factors is depicted in Fig. 7. It can be clearly seen from Fig. 7 that the control energy increases sharply as the assigned square error approaches the minimum value $e_{\min}$. As the square error becomes bigger from near $e_{\min}$, the control energy will decrease remarkably. However, if the given square error is too big, the needed control energy then increases again because more energy is needed to actuate larger generalized displacements. This trend can be observed for any nonlinear coefficients.

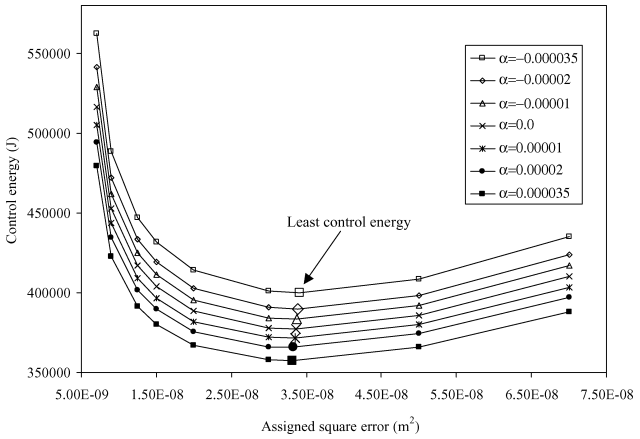

Fig. 7 Relation between the control energy and the constraining square error.

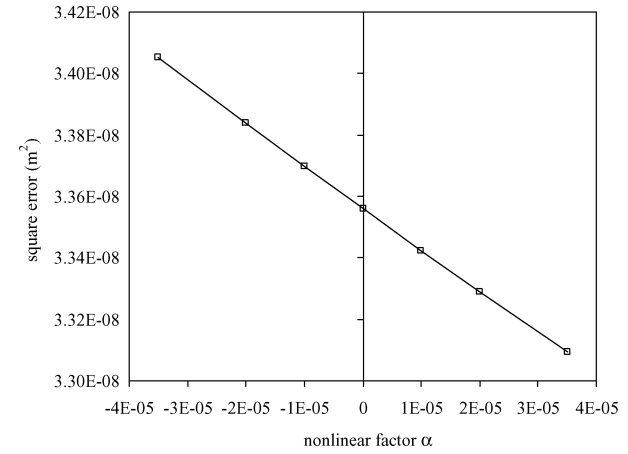

a) Square error via nonlinear factor

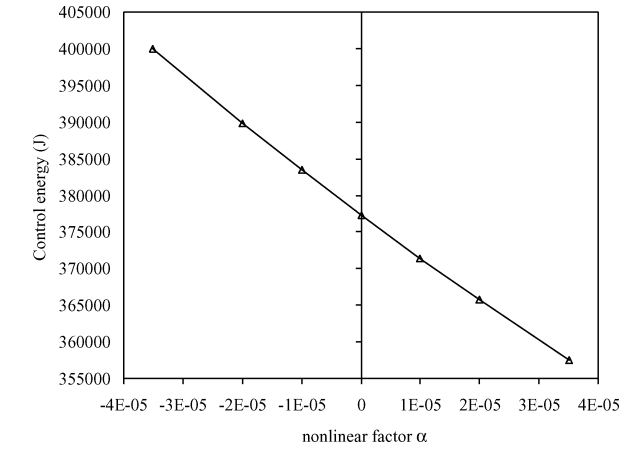

b) Control energy via nonlinear factor

Fig. 8 Effect of the nonlinear factor on ν_{lst} and e_{lst}.

All of the calculations just presented are performed using an equality constraint as given in Eq. (12b). We are more interested in the case where the constraint is an inequality as described in Eq. (12a). As shown in Fig. 7, when $e_0 \leq e_{\text{lst}}$, the energy-constraining square error curve is decreasing monotonously, but it is increasing monotonously when $e_0 > e_{\text{lst}}$. Therefore, if $e_0 \leq e_{\text{lst}}$, the obtained optimal control voltages obtained from Eq. (12b) is the right answer. However, if $e_0 > e_{\text{lst}}$, the right control voltages should be $\boldsymbol{\nu}_{\text{lst}}$ obtained from Eq. (39) because the control energy corresponding to $\boldsymbol{\nu}_{\text{lst}}$ is smallest and the square error actuated by it satisfies the given constraints. In this case, it is critical to find e_{lst} and the corresponding control voltage $\boldsymbol{\nu}_{\text{lst}}$ first, which can be solved from Eq. (30). The $\boldsymbol{\nu}_{\text{lst}}$ and e_{lst} for different nonlinear factors are shown in Fig. 7 using bigger markers. It is found that the square error e_{lst} at which the control voltage distribution has least control energy depends on the nonlinear behavior of the piezoelectric material. Figure 8 shows the effect of the nonlinear factor on $\boldsymbol{\nu}_{\text{lst}}$ and e_{lst}, respectively. It can be seen from Fig. 8 that both the least control energy and its corresponding square error decrease as the nonlinear factor increases. For example, increasing the nonlinear factor from 0 to 0.000035 will lead to a 5.2 and 1.4% reduction in the least control energy and its corresponding square error, respectively. This is because a piezoelectric with higher nonlinear factor can produce more actuating force with same control voltage, as indicated in Fig. 3.

V. Conclusions

Local static shape control of structures integrated with nonlinear piezoelectric actuators using minimum control energy is investigated in this paper. The control energy of the voltage distribution is optimized by imposing two constraints: one is a linear constraint to keep the displacements at the given part as the given values, and the other is an inequality to limit the shape distortion of the residual parts into the assigned error tolerance. An efficient algorithm is presented based on Lagrange multiplier and matrix transformation for finding the optimal voltage distribution for the nonlinear piezoelectric actuator patches. Because repeated calculation of inverse matrix is replacement by solving eigenvalue once in the root-seeking process, this algorithm is very efficient. Simulation results show that both the assigned error tolerance for the residual part and the nonlinear behavior can significantly affect the optimal control voltage distribution as well as the optimal control energy.

Acknowledgment

The authors are grateful for the support of the Australian Research Council via a Discovery-Projects Grant (Grant DP0210716).

References

[1]Haftka, R. T., and Adelman, H. M., "An Analytical Investigation of Shape Control of Large Space Structures by Applied Temperatures," *AIAA Journal*, Vol. 23, No. 3, 1985, pp. 450–457.

[2]Utku, S., Ramesh, A. V., Das, S. K., Wada, B. K., and Chen, G. S., "Control of a Slow-Moving Space Crane as an Adaptive Structure," *AIAA Journal*, Vol. 29, No. 6, 1991, pp. 961–967.

[3]Tolson, R. H., and Huang, J. K., "Integrated Control of Thermally Distorted Large Space Antennas," *Journal of Guidance, Control, and Dynamics*, Vol. 15, No. 3, 1992, pp. 605–614.

[4]Paradies, R., Hertwig, M., and Elspass, W. J., "Shape Control of an Adaptive Mirror at Different Angles of Inclination," *Journal of Intelligent Material Systems and Structures*, Vol. 7, No. 2, 1996, pp. 203–210.

[5]Ericsson, A. J., Bainum, P. M., and Xing, G. Q., "The Optimal LQR Digital-Control of a Free-Free Orbiting Platform," *Acta Astronautica*, Vol. 29, No. 2, 1993, pp. 69–81.

[6]Austin, F., Rossi, M. J., Vannostrand, W., Knowles, G., and Jameson, A., "Static Shape Control for Adaptive Wings," *AIAA Journal*, Vol. 32, No. 9, 1994, pp. 1895–1901.

[7]Agrawal, S. K., Tong, D. Q., and Nagaraja, K., "Modeling and Shape Control of Piezoelectric Actuator Embedded Elastic Plates," *Journal of Intelligent Material Systems and Structures*, Vol. 5, No. 4, 1994, pp. 514–521.

[8]Ghosh, K. G., and Batra, R. C., "Shape Control of Plates Using Piezoceramic Elements," *AIAA Journal*, Vol. 33, No. 7, 1995, pp. 1354–1357.

[9]Bruch, J. C., Sloss, J. M., Adali, S., and Sadek, I. S., "Optimal Piezo-Actuator Locations/Lengths and Applied Voltage for Shape Control of Beams," *Smart Materials and Structures*, Vol. 9, No. 2, 2000, pp. 205–211.

[10]Yang, S. Y., and Ngoi, B., "Shape Control of Beams by Piezoelectric Actuators," *AIAA Journal*, Vol. 38, No. 12, 2000, pp. 2292–2298.

[11]Koconis, D. B., Kollar, L. P., and Springer, G. S., "Shape Control of Composite Plates and Shells with Embedded Actuators. 2. Desired Shape Specified," *Journal of Composite Materials*, Vol. 28, No. 5, 1994, pp. 459–482.

[12]Hsu, C. Y., Lin, C. C., and Gaul, L., "Shape Control of Composite Plates by Bonded Actuators with High Performance Configuration," *Journal of Reinforced Plastics and Composites*, Vol. 16, No. 18, 1997, pp. 1692–1710.

[13]Agrawal, B. N., and Treanor, K. E., "Shape Control of a Beam Using Piezoelectric Actuators," *Smart Materials and Structures*, Vol. 8, No. 6, 1999, pp. 729–739.

[14]Irschik, H., "A Review on Static and Dynamic Shape Control of Structures by Piezoelectric Actuation," *Engineering Structures*, Vol. 24, No. 1, 2002, pp. 5–11.

[15]Park, S. E., and Shrout, T. R., "Ultrahigh Strain and Piezoelectric Behavior in Relaxor-Based Ferroelectric Single Crystals," *Journal of Applied Physics*, Vol. 82, No. 4, 1997, pp.1804–1811.

[16]Zhou, Y. H., and Tzou, H. S., "Active Control of Nonlinear Piezoelectric Circular Shallow Spherical Shells," *International Journal of Solids and Structures*, Vol. 37, No. 12, 2000, pp. 1663–1677.

[17]Ajit, A., Ang, K. K., and Wang, C. M., "Shape Control Coupled Nonlinear Piezoelectric Beams," *Smart Materials and Structures*, Vol. 10, No. 5, 2001, pp. 914–924.

[18]Sun, D. C., Tong, L. Y., and Wang, D. J., "An Incremental Algorithm for Static Shape Control of Smart Structures with Nonlinear Piezoelectric Actuators," *International Journal of Solids and Structures*, Vol. 41, No. 9–10, 2004, pp. 2277–2292.

[19]Crawley, E. F., and Lazarus, K. B., "Induced Strain Actuation of Isotropic and Anisotropic Plates," *AIAA Journal*, Vol. 29, No. 6, 1991, pp. 944–951.

[20]Chee, C. Y. K., Tong, L. Y., and Steven, G. P., "Static Shape Control of Composite Plates Using a Curvature-Displacement Based Algorithm," *International Journal of Solids and Structures*, Vol. 38, No. 36–37, 2001, pp. 6381–6403.

M. Ahmadian
Associate Editor